

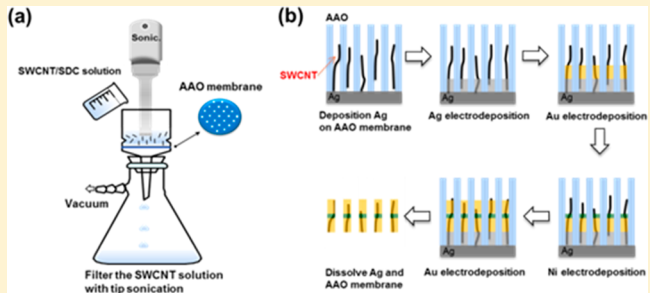
Single-Bundle Carbon-Nanotube-Bridged Nanorod Devices with Control of Gap Length

Gwang-Hyeon Nam, Jae-Hyeok Lee, Nur Elida M. Zahari, Najeeb Choolakadavil Khalid,[†]
Won-Seok Kang, and Jae-Ho Kim*

Department of Molecular Science and Technology, Ajou University, Suwon 443-749, Korea

Supporting Information

ABSTRACT: We report a convenient method for the mass production of single-bundle carbon-nanotube (CNT)-bridged nanorod structures with controlled nanoscale gap. In this research, multisegmented metal nanorods are electrochemically grown on the surface of CNTs that are vertically aligned at inside the pores of anodic aluminum oxide membrane. Selective etching of central nickel (Ni) metal nanorod among three nanorod segments (Au–Ni–Au) provides nanodevice structures with CNT channel in the middle bringing between metal nanorod electrodes on both ends. Our method offers a simple pathway for production of nanoscale gap controlled CNT based devices with desired length of both channel and electrodes. This CNT-bridged nanorod structure holds advantages of each constituent, including the electrical properties of CNTs such as a ambipolar characteristic, and precise growth control and alignment of nanorods. This method provides an easy and convenient approach to fabricate various kinds of nanoscale structure-based electronic devices.



INTRODUCTION

A nanoscale gap device has emerged as an excellent candidate for the nanoelectronics and sensor applications.^{1–4} A wide range of one-dimensional (1D) nanostructured materials^{5,6} such as nanorods,^{7–12} nanowires,^{13,14} nanobelts,^{15,16} and nanotubes^{17–22} have shown capabilities for the fabrication of devices. In particular, the 1D structure of carbon nanotubes (CNTs) and its high current mobility make them suitable candidate to overcome fundamental limitations of silicon-based metal-oxide-semiconductor (MOS) electronics such as device performance and complex fabrication process.^{23,24} These nanostructured materials also can be easily tailored as conducting channels due to the long axis of their structure in electric devices. In biosensors as one area of versatile applications, target materials such as biomolecules²⁵ can attach on the sensing devices and transmit signals in the form of resistance, capacitance, and conductance.²⁶ Especially, CNTs are prominent to detect chemical and biological materials due to its small diameter and local gate sensitivity, allowing more signal transfer in the device.

In spite of the potential and advances of nanomaterials in the field of nanoelectronic devices, some crucial issues remain as challenges in the same manner with arrangement,²⁷ alignment,^{28,29} stable contact with electrodes,³⁰ and control of gap distance.³¹ These issues highly rely on the fabrication technique. Many research groups have used a combination of two or more fabrication methods so as to overcome the drawback of each fabrication technique. Researchers achieved the nanodevice fabrication through the direct writing

techniques such as e-beam lithography and dip-pen lithography (DPN) by making nanometer-scale patterns.³² Dielectrophoresis with breakdown technique also has shown to provide simple and less time-consuming production of the CNT-field effect transistor (FET).^{33,34} In combination techniques, diverse nanodevices were achieved as mentioned above, but there are technical problems to be surmounted like long process time which makes it difficult to use for mass production or limitations to provide the specific size control.

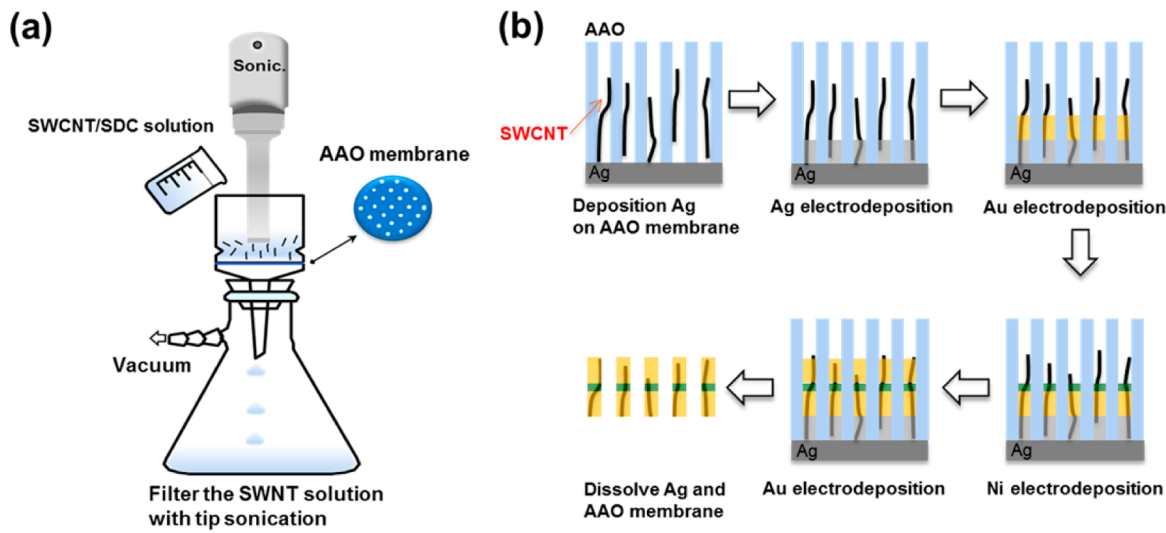
Among various techniques available, one of them for fabricating the single-walled carbon nanotube (SWCNT) device is the electrochemical deposition method using anodized aluminum oxide (AAO) channel. For example, Ou et al. reported a combination technique of CVD and on-wire lithography (OWL)³⁵ for CNT devices.³⁶ However, the diameters of SWCNTs are depending upon the pore size of the template and the common pore size is in micrometer scale. Recently, Lee et al. reported CNT-bridge wires with a gap distance of 5 nm and average diameter of 360 ± 20 nm.³⁷ Smaller gap distance gives rise to low resistivity due to high flow of electrical charges through the material, which is an important characteristic for high sensitivity and efficiency of nanodevice.²⁷ The mass production of devices is another hurdle since it is difficult to control the SWCNTs diameter and the gap distance between the SWCNTs and electrodes. Therefore,

Received: February 23, 2014

Revised: April 4, 2014

Published: April 9, 2014

Scheme 1. (a) Simultaneous Process of Filtration and Ultrasonication of SWCNT–SDC Solution; (b) Preparation of Multisegment Nanorod on the SWCNTs Vertically Suspended inside AAO Pores



well-designed and optimized experimental conditions are crucial for the effective fabrication of nanoelectronic devices and applications.

Herein, we demonstrate a cost-effective and straightforward production of single-bundle CNT-bridged nanorod structures via a combination of techniques which are vacuum filtration with a simultaneous ultrasound sonication method, OWL, and most importantly the surface engineering of SWCNTs. The property of CNTs assigned by this surface engineering allows CNTs to be efficient for infiltration into AAO pore and fabrication of single-bundle CNT-bridged nanorod devices. The single CNT bundle as a conducting channel enables CNT-bridged nanorod devices to use as the FET or various applications. And also, the advantage of this combination technique is the efficient method to position and align SWCNTs inside the AAO channel, which enables a mass production of CNT-bridged nanorod structures with gap control.

EXPERIMENTAL SECTION

Preparation of SWCNT Dispersion. The CNTs used in this study are arc-discharge SWCNTs (HANOS Hanwha Nanotech, Korea), and the selected surfactant is sodium deoxycholate (SDC, Sigma-Aldrich). First, 2% SDC was dissolved in deionized (DI) water. After that, 10 mg of SWCNTs was added and sonicated (Vibra Cell VC) at 500 W for 1 h in an ice bath. Ice–water cooling was used throughout the sonication process in order to prevent heating of the sample. Then, the solution was centrifuged at 15 000 rpm for 1 h to purify monodispersed SWCNTs. Well-dispersed nanotubes were obtained by collecting the supernatant solution. From this stock solution, 15 mL of the stock solution was diluted into 400 mL with DI water.

Infiltration and Alignment of SWCNTs inside AAO Channel. The most challenging part in this experiment is the process of placing and aligning SWCNTs inside the AAO channel (200 nm, Anodisc, Whatman Inc.). The basic step for this process is to filter the SWCNTs solution via AAO as the SWCNTs that entered into the AAO were attached to the AAO wall. During the filtration process, the nanotubes tend to randomly sediment on the top of AAO channel and form thin

layer of SWCNTs network (Figure S3 in the Supporting Information). This sedimentation layer blocks the AAO channel, forbidding the remaining SWCNTs from entering the channels. Since the wave from a tip sonicator is able to detach SWCNTs on the sediment layer, ultrasonication and vacuum filtration were conducted simultaneously to improve the efficiency of CNT penetration into AAO pore.

Nanorod Fabrication. The fabrication of this structure was implemented by electrodeposition method of three different metals inside the pores of the AAO membrane (200 nm, Anodisc, Whatman Inc.). The AAO membrane used in the previous step was prepared in this process. The plating solutions of Ag, Au, and Ni were obtained from Technic Inc. The structure of SWCNT device depends on the geometrical size and shape of the AAO membrane, i.e., average channel diameter of 200 nm and length of 60 μm . At first, a 300 nm thick Ag layer was deposited by an ion coater (IB-3, Eiko Engineering Co., Ltd., Japan) on the AAO membrane to seal the pores and to perform it as working electrode in a three-electrode electrodeposition system (BAS 100, BASi). The reference and counter electrodes were Ag/AgCl and platinum wire, respectively. A Teflon cell was assembled by using a O-ring to avoid the leakage of the plating solutions. The plating reduction of metal ions in the sequence of Ag, Au, Ni, and Au was carried out to prepare a multisegment nanorod. The length of the nanorod in the membrane channel was controlled by the amount of electric charge passing through the circuit. The Ag nanorod was potentiostatically deposited at -750 mV from a commercial plating solution (Techni Silver 1025 RTU). The Au (Orotemp 24 RTU) and Ni (Nickel Sulfamate RTU) segments were electrochemically deposited at -850 and -900 mV, respectively. After completely growing the multisegment nanorod, the AAO membrane was immersed in HNO_3 in order to remove the Ag used as a working electrode followed by dissolving AAO membrane in a 3 M NaOH aqueous solution. After that, the multisegment nanorod was separated by centrifugation in DI water and finally with ethanol solvent. The single-bundle CNT-bridged nanorods solution was drop-casted on a Si/SiO₂ wafer (p type, 1–10 $\Omega\cdot\text{cm}$). The single-bundle CNT-bridged nanorod devices were provided by

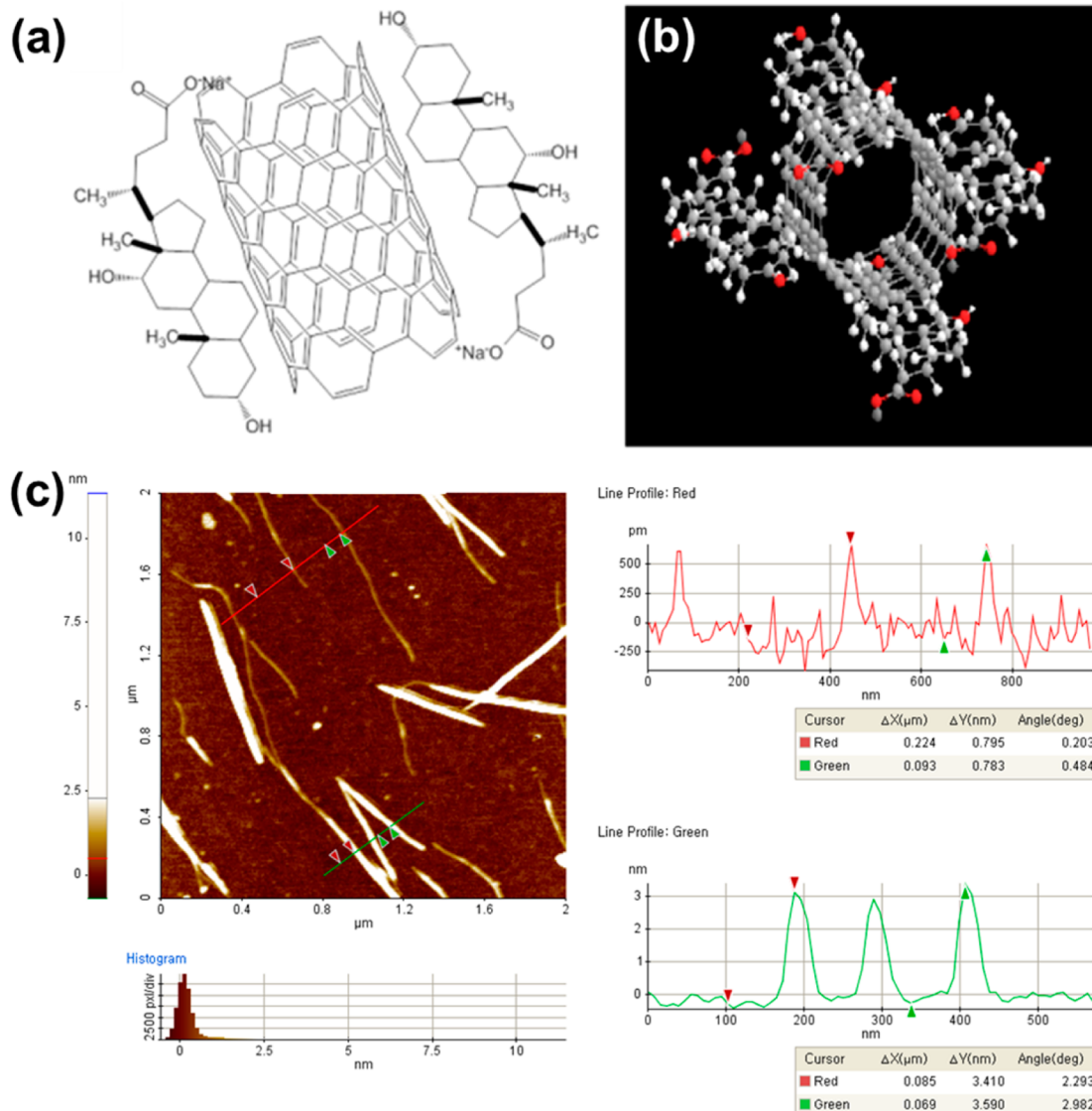


Figure 1. (a) Schematic representation of the SDCs adsorbed on SWCNT and (b) a ball-and-stick model of the same. (c) AFM image of the SWCNTs with SDC adsorbed on its surface. The red line shows the line profile of the individual SWCNTs (diameter: 0.8 nm). The green line shows the line profile of the SWCNT bundles (diameter: 3.5 nm).

selective chemical wet etching of central Ni nanorod portions (30% FeCl_3). The wafer was heated to 60 °C for 30 min.

Characterization. The surface structure and dimension of CNT-bridged nanorods are characterized by using a field emission scanning electron microscope (FE-SEM, LEO SUPRA 55, Carl Zeiss NTS GmgH, Germany) operating at 10 kV. All atomic force microscopy (AFM) images were performed on a XE-100 AFM system (Park Systems Corp., Korea) in noncontact mode. The cantilever used an ARROW-NCR-50 noncontact cantilever (NanoWorld Corp., Switzerland). The typical spring constant and the resonance frequency were 42 N/m and 285 kHz, respectively. In order to confirm the existence and properties of SWCNTs between the nanorod, micro-Raman spectroscopy analysis was conducted (632 nm He:Ne laser, inVia Raman microscope, Renishaw). $I-V$ curves and two-probe resistances of CNT-bridged nanorod devices were measured with a Keithly 2612 semiconductor parameter analyzer.

RESULTS AND DISCUSSION

Scheme 1 shows the experimental procedure involved in the preparation of multisegment nanorods. Our approach is based on utilization of SWCNTs in a modified OWL. In this study, the SWCNTs were dispersed with the assistance of sodium deoxycholate (SDC). The solution was filtered through an AAO membrane with pore size of 200 nm under a simultaneous probe sonication. Through this process, the SWCNTs were affixed to the side walls of the AAO membrane (Figure S1 in the Supporting Information). The AAO membrane with the adsorbed SWCNTs was used as a template to grow nanorods, as illustrated in Scheme 1. Multisegmented nanorods (Au–Ni–Au) were electrochemically grown on the SWCNTs that are adsorbed inside the AAO pores. After removing the AAO template using 3 M aqueous sodium hydroxide (NaOH) solution, followed by 30% FeCl_3 etching of the central Ni nanorod provided CNT-bridged nanorod devices. The length of Ni nanorods was designed to obtain the nanorod devices with various gaps.

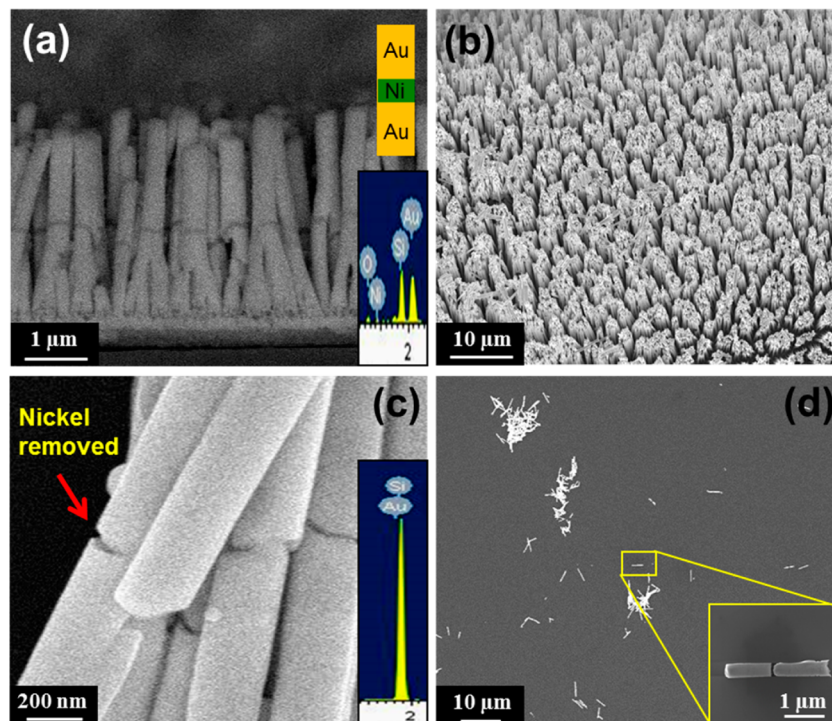


Figure 2. SEM images of nanoscale gap SWCNTs. (a) Free-standing multisegment nanorod Au–Ni–Au after removing the AAO membrane. The inset image is EDS data demonstrating multisegment rods consists of Ni and Au. (b) Mass production of multisegment nanorod. (c) Empty layer or gap at multisegment rods after removing the Ni. The inset image is the EDS analysis demonstrating the presence of Au. (d) Multisegment nanorod drop deposited on Si wafer. Enlarged image reveals the presence of SWCNTs.

In this method, there are two major factors that affect the formation of the single-bundle CNT-bridged nanorod structure: first, the condition for filtering the SWCNT solution through the AAO membrane; second, the physical property of the SWCNTs with SDC. When the dispersion is filtered through the AAO template, normally SWCNTs assemble into a sedimentary layer on the template. Once deposited, this sedimentary layer accumulates without removal during filtration. Therefore, the possibility of CNT penetration into pore is low since this layer blocks the pores. Eventually, the SWCNTs cannot attach on the sidewall of the AAO pores, or only a few nanotubes adhere to the surface. But, when the dispersion is filtered with simultaneous tip sonication, the sedimentary SWCNTs are detached from the AAO membrane surface, and they are able to infiltrate into the pores. Through tip sonication, a clearer AAO surface can explain this point after filtering CNT solution (Figure S2 in the Supporting Information). Considering the second factor, it is important to arrange single-bundle CNT that surface engineering with SDC is designed to equip CNTs for rigidity. SDC contributions are discussed in detail below. The straightness of CNT is maintained in fabrication process. If the materials are bent in the pores, it is possible for the CNTs to connect double or more junctions with Au nanorod. Moreover, this distorted structure influence electrical properties of CNTs.³⁸ To eliminate these variations for device properties, we designed single-bundle structure.

Figures 1a and 1b show schematics of the SWCNT with the affixed SDCs on surface. The SDC has a hydrophobic region comprising a steroid-ring structure and a hydrophilic region of a charged carboxyl group. In water, the hydrophobic region of the SDC makes contact with the surface through the hydrophobic interaction. This interaction even makes a

compact layer of cholate ions on the surface due to the rigidity of the steroid-ring structure of the SC.³⁹ The compact SDC layer on the SWCNT prevents it from bending (Figure S3 in the Supporting Information). Thus, the surface modification of the SWCNTs with SDC provides the SWCNTs with a rigid property due to the presence of the compact steroid-ring structure layer (Figure 1c). Therefore, our methodologies effectively resolved the aforementioned problems associated with the adsorption of the single-bundle CNTs inside the AAO pores.

In order to control the nanogap distance, multisegment nanorods were fabricated with various different length of Ni nanorod. The length of Ni nanorod was controlled by varying amount of charge applied during the electrochemical deposition process. The fabrication process is depicted Scheme 1 with nanoscale gap controlled CNT-bridged structure. The dimension of the device is based on the geometrical size and shape of the AAO membranes. The plating of metal salts Au, Ni, and then Au is carried out sequentially to prepare multisegment nanorod. The length of the nanorod is controlled by the amount of electric charge passing through the circuit in the channels. The SEM image of multisegment nanorods of Au–Ni–Au that are grown by the template approach is shown in Figure 2. The darker layer in the image is representing the Ni metal, and the other layers are Au nanorods. To confirm the absence and the identifications of multi segment nanorods, characterization was conducted by energy dispersive X-ray spectroscopy (EDS). The EDS spectrum of nanorod was taken before removing Ni segments and detected the Ni peak (Figure 2a, inset). Only Si and Au peaks were remained after chemically etching the Ni segments (the Ni peak disappeared, Figure 2c, inset). After fabricating the multisegment nanorod, it was drop deposited on silicon oxide wafer. The Ni layer was removed by

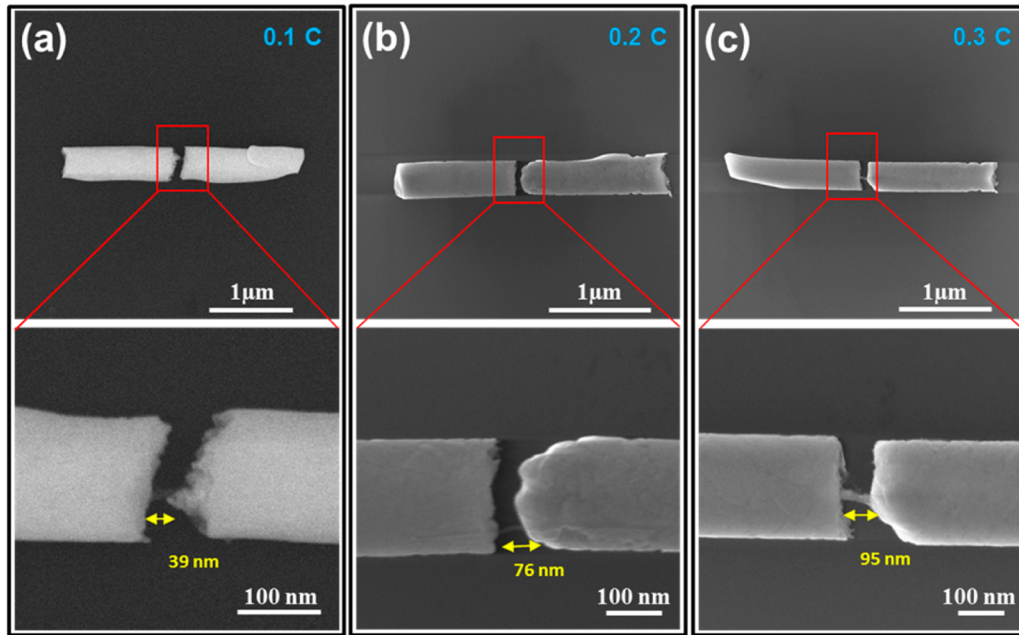


Figure 3. SEM images of nanogap devices with three different SWCNT bridge distances: (a) 39, (b) 76, and (c) 95 nm.

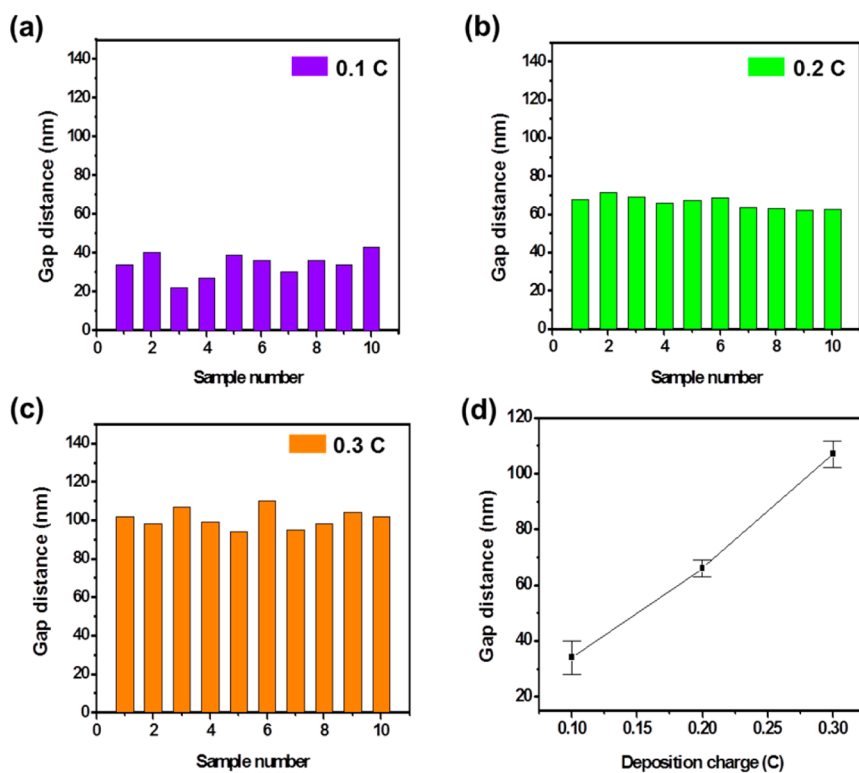


Figure 4. (a) SWCNT device gap at different electrochemical deposition charges: (a) 0.1, (b) 0.2, and (c) 0.3 C. (d) Graph of charge versus gap distance.

30% FeCl_3 , leaving empty space or gap distance between both Au nanorods. Through this process, single-bundle CNT-bridged nanorod devices were successfully fabricated with various channel length.

The SEM images in Figure 3 demonstrate that the smallest gap is 39 nm, which was obtained when the Ni layer was grown at a 0.1 C of charge. The gap sizes of 76 and 95 nm were obtained at deposition 0.2 and 0.3 C of charge, respectively. These gap values have almost constant increment as displayed

in Figure 4a. In this graph, when the deposition charge is increasing from 0.1 to 0.3 C, the length of Ni nanorod relatively became longer and consequently indicates the SWCNT device gap are also extended. Ten measurements of gap distances were collected and the average gap sizes were found to be 34 ± 6 , 66 ± 3 , and 107 ± 5 nm at 0.1, 0.2, and 0.3 C, respectively. It can be clearly seen in the SEM image that there is a SWCNT bundle exist in the gap, and the bundle is connected to the surface of the Au nanorods at both ends. This provides the

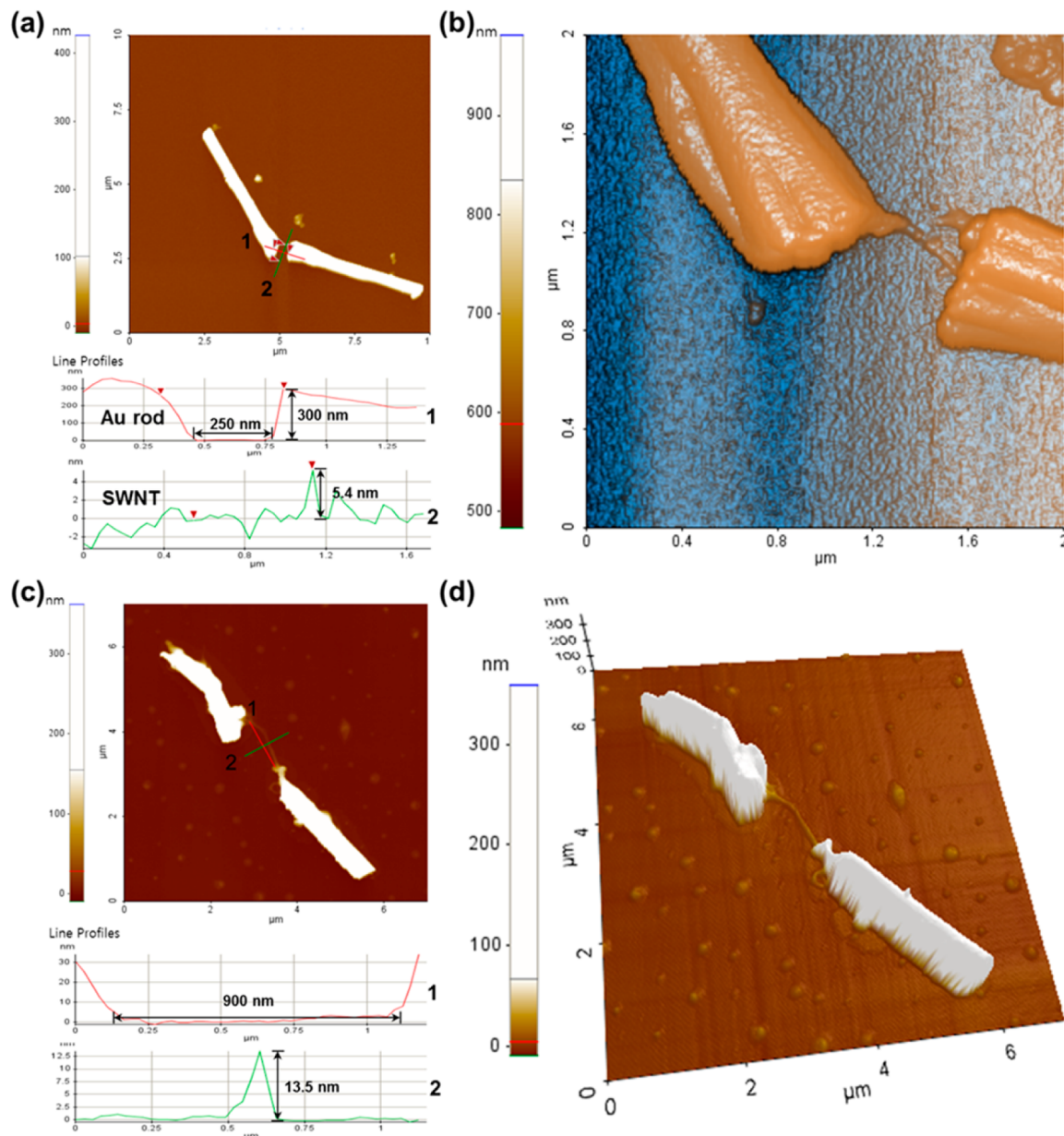


Figure 5. Confirmation of SWCNTs at the nanogap using AFM. Devices constructed with different lengths of Au and Ni nanorods. (a) Length of Au nanorod: 4 μm , Ni nanorod: 250 nm and (b) enlarged 3D AFM image of the same device. (c) Length of Au nanorod: 2.5 μm , Ni nanorod: 900 nm and (d) enlarged 3D AFM image of the same device.

evidence to prove that a single bundle CNT-bridged nanorod was fabricated after the SWCNTs were adsorbed in the interior of the AAO wall. The characterizations of the SWCNTs presents in the nanogaps were conducted by AFM and micro-Raman spectroscopy.

To clearly measure the CNT bundle between Au nanorods by AFM, we prepared the single-bundle CNT-bridged nanorod devices with long gaps (250 and 900 nm) by tailoring the length of the middle Ni nanorod segment. Figures 5a and 5b show the AFM image and line profiles of the single-bundle SWCNT-bridged nanorod. It was fabricated using an AAO template through which 0.1 and 0.5 mg/L SWCNT solutions were filtered. In Figure 5a, the structure possesses a gap of 250 nm, and the diameter of the bundle is 5.4 nm in the gap. The gap in Figure 5b shows a CNT-bridged nanorod structure with a gap of 900 nm and SWCNT bundle diameter of 13.5 nm. The

SWCNT bundle has a bigger bundle diameter in nanorod device than that in the device shown in Figure 5b. This is because concentration of the dispersion influences the bundle size of CNTs. These results show that concentration of the dispersion influences the diameter of the bundle. In other words, conducting channel width was controlled by concentration. Stability is another important factor in these structures. Although the CNT-bridged nanorods were cast on a silicon substrate after a process, such as centrifugation, sonication, or selective etching for the Ni nanorod, they sustained a SWCNT-bridged nanorod form with a single bundle. Accordingly, it is clear that SWCNTs are strongly connected with Au nanorods, and the structure is stable.

We characterized the SWCNTs exist in the single-bundle SWCNT-bridged nanorod by using a micro-Raman spectro-

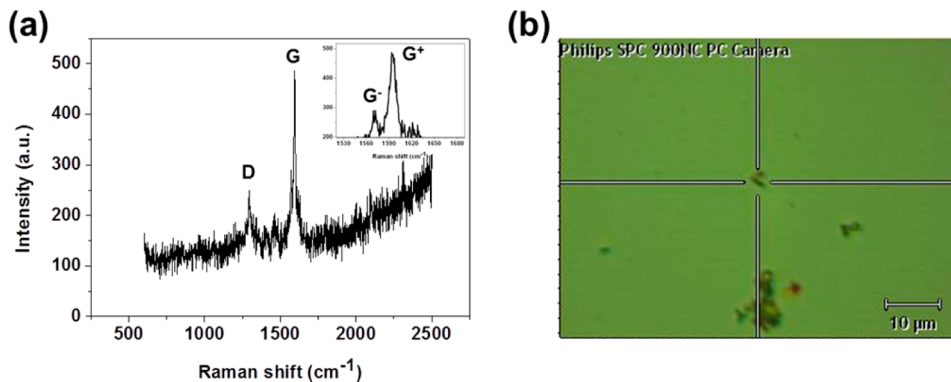


Figure 6. (a) Raman spectrum of an SWCNT-bridged nanorod. The inset is a magnification of the G-band. (b) The optical microscopic image of an SWCNT-bridged nanorod measured with the Raman spectrometer.

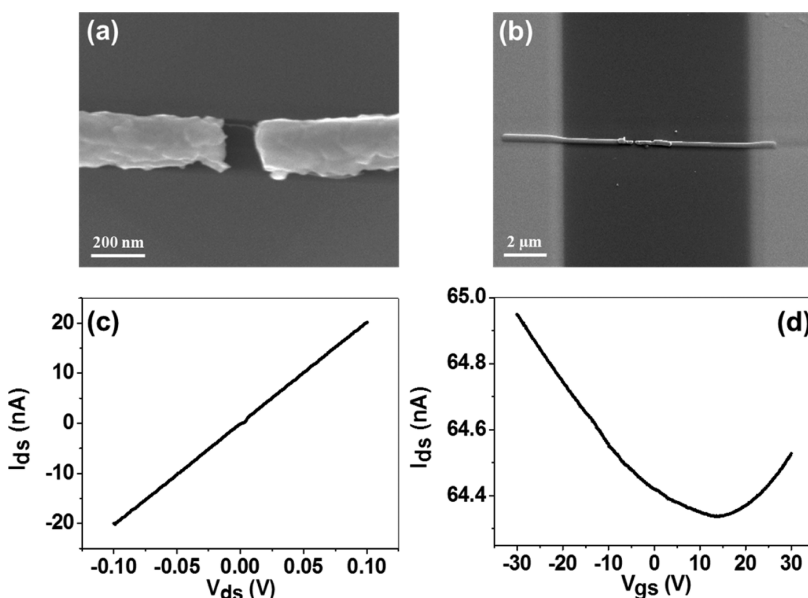


Figure 7. SEM images of the SWCNT-bridged nanorod before Pt electrode deposition (a) and after (b). (c) Plot of the drain-source current (I_{ds}) versus the drain-source voltage (V_{ds}) for an SWCNT-bridged nanorod at room temperature. (d) Plot of the drain-source current (I_{ds}) versus the gate-source voltage (V_{gs}) for an SWCNT-bridged nanorod. The bias voltage is 0.3 V.

scope. The Raman signal showed two characteristic peaks (Figure 6), such as D-band and G-band at 1293 and 1592 cm^{-1} , respectively. The G/D ratio of this SWCNT-bridged nanorod was 3.1. The value was lower than that of general research, but this result does not mean that the quality of the SWCNT was poor. The spot size of the micro-Raman was too big to measure the bridged nanotubes only. The value of the nanotube buried in the Au electrode part was inhibited the lattice vibration. Therefore, this G/D ratio reflected the Raman signal of the SWCNTs buried in the Au and suspended in air. The G-band at 1592 cm^{-1} showed two dominant Lorentzian features, which means that the CNTs of this device possesses semiconducting nanotubes.⁴⁰

Finally, the electrical properties of CNT-bridged nanorods were evaluated as follows. We fabricated a three-terminal device with the single bundle CNT-bridged nanorod device by depositing platinum (Pt) electrodes by using e-beam lithography (Figure S4 in the Supporting Information). The Si/SiO₂ substrate was used as a back gate and thermally grew 500 nm thick SiO₂ as gate dielectrics. This device had a channel length of 100 nm and proper Ohmic junction. Figures 7a and 7b show the FET characteristic of a single-bundle CNT-bridged

nanorod device at room temperature with the on current (I_{on}) of ~60 nA and a linear on-state resistance (R_{on}) of 1667 kΩ at a bias voltage of 0.3 V. The CNT-bridged nanorod device shows the ambipolar property due to the adsorbed oxygen at ambient conditions and 14 V of Dirac point resulting from a gate sweep. This result is consistent with Bisiri's report that the shift of threshold voltage is attributed to deep electron traps from oxygen doping effect.⁴¹ The exposure of semiconducting SWCNTs (sSWCNTs) to oxygen and water moisture can induce hole doping and electron trapping. The oxygen/water redox couple could electrochemically induce electron transfer from sSWCNTs and suppress electron conduction. This contributes to the deep electron traps that shift the V_{Th} for electrons. The on-off ratio of the device was low. This result was induced since the single bundle, as a conducting channel, was suspended in air. The relative permittivity of air (1.0) is approximately 4-fold lower than silicon dioxide (3.9).⁴² Thus, the device showed a low on-off ratio because the SWCNT bundle suspended in air was weakly influenced by the electric field.

CONCLUSIONS

We fabricated single-bundle CNT-bridged nanorod devices using combination of techniques: vacuum filtration of SWCNT solution through AAO membrane with a simultaneous ultrasonication followed by the OWL. The surface treatment of SWCNTs with SDC influenced the physical property of the SWCNTs, and the rigidity of the SWCNTs enabled effective adsorption of single-bundle SWCNTs in the interior of AAO side wall and CNT distortion. Our CNT-bridged nanorod device fabrication approach offers the possibility of fabrication of devices consisting of a few CNTs cost effectively and without need for highly sophisticated techniques. The channel length of the device can be easily adjusted by controlling the nanorod growth. This is a high-yield fabrication method when compared to other conventional methods because many nanorods can grow simultaneously in a number of pores of AAO, and therefore numerous single bundle CNT-bridged nanorods can be formed at a time. It is possible to apply this structure in various semiconducting devices, such as FETs, chemical or biosensors. Moreover, this method can be applied to materials similar to SWCNTs, which also have a rigid property. Thus, it would be possible to provide an easy approach to evaluating semiconducting materials in electronics.

ASSOCIATED CONTENT

Supporting Information

Figures S1–S4. This material is available free of charge via the Internet at <http://pubs.acs.org>.

AUTHOR INFORMATION

Corresponding Author

*E-mail: jhkim@ajou.ac.kr (J.-H.K.).

Present Address

[†]N.C.K.: Hanbang Skincare Research Team, Amorepacific R&D center, Gyeonggi-do, Yongin, 446-729, Republic of Korea.

Notes

The authors declare no competing financial interest.

ACKNOWLEDGMENTS

This research was supported by Basic Science Research Program through the National Research Foundation of Korea (NRF) funded by the Ministry of Education (No. 2009-0093826). In addition, we thank the BK21 Program of Molecular Science and Technology at Ajou University.

REFERENCES

- (1) Li, T.; Hu, W.; Zhu, D. Nanogap Electrodes. *Adv. Mater.* **2010**, *22*, 286–300.
- (2) Cui, Y.; Wei, Q.; Park, H.; Lieber, C. M. Nanowire Nanosensors for Highly Sensitive and Selective Detection of Biological and Chemical Species. *Science* **2001**, *293*, 1289–1292.
- (3) Xia, Y.; Yang, P.; Sun, Y.; Wu, Y.; Mayers, B.; Gates, B.; Yin, Y.; Kim, F.; Yan, H. One-Dimensional Nanostructures: Synthesis, Characterization, and Application. *Adv. Mater.* **2003**, *15*, 353–398.
- (4) Storm, K.; Nylund, G.; Samuelson, L.; Micolich, A. P. Realizing Lateral Wrap-Gated Nanowire FETs: Controlling Gate Length with Chemistry Rather than Lithography. *Nano Lett.* **2012**, *12*, 1–6.
- (5) Kuchibhatla, S. V. N. T.; Karakoti, A. S.; Bera, D.; Seal, S. One Dimensional Nanostructured Materials. *Prog. Mater. Sci.* **2007**, *52*, 699–913.
- (6) Yuan, J.; Xu, Y.; Müller, A. H. E. One-Dimensional Magnetic Inorganic–Organic Hybrid Nanomaterials. *Chem. Soc. Rev.* **2011**, *40*, 640–655.
- (7) Kim, L.; Kim, J.; Gu, G. H.; Suh, J. S. Fabrication of Well-Ordered Molecular Device Arrays. *Chem. Phys. Lett.* **2006**, *427*, 137–141.
- (8) Chen, N.; Huang, C.; Yang, W.; Chen, S.; Liu, H.; Li, Y.; Li, Y. Growth Control for Architecture Molecular Conductor of Low Dimension Nanostructures. *J. Phys. Chem. C* **2010**, *114*, 12982–12986.
- (9) Pedano, M. L.; Li, S.; Schatz, G. C.; Mirkin, C. A. Periodic Electric Field Enhancement along Gold Rods with Nanogaps. *Angew. Chem., Int. Ed.* **2010**, *49*, 78–82.
- (10) Pedano, M. L.; Li, S.; Schatz, G. C.; Mirkin, C. A. Designing, Fabricating, and Imaging Raman Hot Spots. *Proc. Natl. Acad. Sci. U. S. A.* **2006**, *103*, 13300–13303.
- (11) Osberg, K. D.; Schmucker, A. L.; Senesi, A. J.; Mirkin, C. A. One-Dimensional Nanorod Arrays: Independent Control of Composition, Length, and Interparticle Spacing with Nanometer Precision. *Nano Lett.* **2011**, *11*, 820–824.
- (12) Chen, X.; Jeon, Y. M.; Jang, J. W.; Qin, L.; Huo, F.; Mirkin, C. A. On-Wire Lithography-Generated Molecule-Based Transport Junctions: A New Testbed for Molecular Electronics. *J. Am. Chem. Soc.* **2011**, *130*, 8166–8168.
- (13) Yao, J.; Yan, H.; M. Lieber, C. A Nanoscale Combing Technique for the Large-Scale Assembly of Highly Aligned Nanowires. *Nat. Nanotechnol.* **2013**, *3*, 329–335.
- (14) Tian, B.; Xie, P.; Kempa, T. J.; Bell, D. C.; Lieber, C. M. Single-Crystalline Kinked Semiconductor Nanowire Superstructures. *Nat. Nanotechnol.* **2009**, *4*, 824–829.
- (15) Wang, Z. L. ZnO Nanowire and Nanobelt Platform for Nanotechnology. *Mater. Sci. Eng., R* **2009**, *64*, 33–71.
- (16) Fang, X.; Xiong, S.; Zhai, T.; Bando, Y.; Liao, M.; Gautam, U. K.; Koide, Y.; Zhang, X.; Qian, Y.; Golberg, D. High-Performance Blue/Ultraviolet-Light-Sensitive ZnSe-Nanobelt Photodetectors. *Adv. Mater.* **2009**, *21*, 5016–5021.
- (17) Bandaru, P. R. Electrical Properties and Applications of Carbon Nanotube Structures. *J. Nanosci. Nanotechnol.* **2007**, *7*, 1–29.
- (18) Volder, M. F. L. D.; Tawfick, S. H.; Baughman, R. H.; Hart, A. J. Carbon Nanotubes: Present and Future Commercial Applications. *Science* **2013**, *339*, 535–539.
- (19) Kim, S.; Ju, S.; Back, J. H.; Xuan, Y.; Ye, P. D.; Shim, M.; Janes, D. B.; Mohammadi, S. Fully Transparent Thin-Film Transistors Based on Aligned Carbon Nanotube Arrays and Indium Tin Oxide Electrodes. *Adv. Mater.* **2009**, *21*, 564–568.
- (20) LeMieux, M. C.; Roberts, M.; Barman, S.; Jin, Y. W.; Kim, J. M.; Bao, Z. Self-Sorted, Aligned Nanotube Networks for Thin-Film Transistors. *Science* **2008**, *321*, 101–104.
- (21) Sangwan, V. K.; Ortiz, R. P.; Alaboson, J. M. P.; Emery, J. D.; Bedzyk, M. J.; Lauhon, L. J.; Marks, T. J.; Hersam, M. C. Fundamental Performance Limits of Carbon Nanotube Thin-Film Transistors Achieved Using Hybrid Molecular Dielectrics. *ACS Nano* **2012**, *6*, 7480–7488.
- (22) Engel, M.; Steiner, M.; Sundaram, R. S.; Krupke, R.; Green, A. A.; Hersam, M. C.; Avouris, P. Spatially Resolved Electrostatic Potential and Photocurrent Generation in Carbon Nanotube Array Devices. *ACS Nano* **2012**, *6*, 7303–7310.
- (23) Iijima, S.; Ichihashi, T. Single-Shell Carbon Nanotubes of 1-nm Diameter. *Nature* **1993**, *363*, 603–605.
- (24) Cao, Q.; Rogers, J. A. Ultrathin Films of Single-Walled Carbon Nanotubes for Electronics and Sensors: A Review of Fundamental and Applied Aspects. *Adv. Mater.* **2009**, *21*, 29–53.
- (25) Allen, B. L.; Kichambare, P. D.; Star, A. Carbon Nanotube Field-Effect-Transistor-Based Biosensors. *Adv. Mater.* **2007**, *19*, 1439–1451.
- (26) Meng, F.; Jiang, L.; Zheng, K.; Goh, C. F.; Lim, S.; Hng, H. H.; Ma, J.; Boey, F.; Chen, X. Protein-Based Memristive Nanodevices. *Small* **2011**, *7*, 3016–3020.
- (27) Druzhinina, T. S.; Höppener, C.; Hoeppener, S.; Schubert, U. S. Hierarchical, Guided Self-Assembly of Preselected Carbon Nanotubes

- for the Controlled Fabrication of CNT Structures by Electrooxidative Nanolithography. *Langmuir* **2013**, *29*, 7515–7520.
- (28) Xu, M.; Futaba, D. N.; Yumura, M.; Hata, K. Tailoring Temperature Invariant Viscoelasticity of Carbon Nanotube Material. *Nano Lett.* **2011**, *11*, 3279–3284.
- (29) Xu, M.; Futaba, D. N.; Yumura, M.; Hata, K. Alignment Control of Carbon Nanotube Forest from Random to Nearly Perfectly Aligned by Utilizing the Crowding Effect. *ACS Nano* **2012**, *6*, 5837–5844.
- (30) White, C. T.; Todorov, T. N. Nanotubes Go Ballistic. *Nature* **2001**, *411*, 649–651.
- (31) Wei, D.; Liu, Y.; Cao, L.; Wang, Y.; Zhang, H.; Yu, G. Real Time and in Situ Control of the Gap Size of Nanoelectrodes for Molecular Devices. *Nano Lett.* **2008**, *8*, 1625–1630.
- (32) Wang, W. M.; LeMieux, M. C.; Selvarasah, S.; Dokmeci, M. R.; Bao, Z. Dip-Pen Nanolithography of Electrical Contacts to Single-Walled Carbon Nanotubes. *ACS Nano* **2009**, *11*, 3543–3551.
- (33) Vijayaraghavan, A.; Blatt, S.; Weissenberger, D.; Oron-Carl, M.; Hennrich, F.; Gerthsen, D.; Hahn, H.; Krupke, R. Ultra-Large-Scale Directed Assembly of Single-Walled Carbon Nanotube Devices. *Nano Lett.* **2007**, *7*, 1556–1560.
- (34) Li, J.; Zhang, Q.; Yang, D.; Tian, J. Fabrication of Carbon Nanotube Field Effect Transistors by AC Dielectrophoresis Method. *Carbon* **2004**, *42*, 2263–2267.
- (35) Qin, L.; Park, S.; Huang, L.; Mirkin, C. A. On-Wire Lithography. *Science* **2005**, *309*, 113–115.
- (36) Ou, F. S.; Shajumon, M. M.; Ci, L.; Benicewicz, D.; Vajtai, R.; Ajayan, P. M. Multisegmented One-Dimensional Hybrid Structures of Carbon Nanotubes and Metal Nanowires. *Appl. Phys. Lett.* **2006**, *89*, 243122–1–243122–3.
- (37) Lee, B. Y.; Heo, K.; Schmucker, A. L.; Jin, H. J.; Lim, J. K.; Kim, T.; Lee, H.; Jeon, K. S.; Suh, Y. D.; Mirkin, C. A.; Hong, S. Nanotube-Bridged Wires with Sub-10 nm Gaps. *Nano Lett.* **2012**, *12*, 1879–1884.
- (38) Tombler, T. W.; Zhou, C.; Alexseyev, L.; Kong, J.; Dai, H.; Liu, L.; Jayanthi, C. S.; Tang, M.; Wu, S.-Y. Reversible Electromechanical Characteristics of Carbon Nanotubes Under Local-Probe Manipulation. *Nature* **2000**, *405*, 769–772.
- (39) Lin, S.; Blankschtein, D. Role of the Bile Salt Surfactant Sodium Cholate in Enhancing the Aqueous Dispersion Stability of Single-Walled Carbon Nanotubes: A Molecular Dynamics Simulation Study. *J. Phys. Chem. B* **2010**, *114*, 15616–15625.
- (40) Jishi, R. A.; Venkataraman, L.; Dresselhaus, M. S.; Dresselhaus, G. Phonon Modes in Carbon Nanotubules. *Chem. Phys. Lett.* **1993**, *209*, 77–82.
- (41) Bisri, S. Z.; Gao, J.; Derenskyi, V.; Gomulya, W.; Iezhokin, I.; Gordiichuk, P.; Herrmann, A.; Loi, M. A. High Performance Ambipolar Field-Effect Transistor of Random Network Carbon Nanotubes. *Adv. Mater.* **2012**, *24*, 6147–6152.
- (42) Gray, P. R. In *Analysis and Design of Analog Integrated Circuits*, 5th ed.; Hurst, P. J., Lewis, S. H., Meyer, R. G., Eds.; Wiley: New York, 2009; p 156.